Supporting Information

Axup et al. 10.1073/pnas.1211023109

SI Materials and Methods

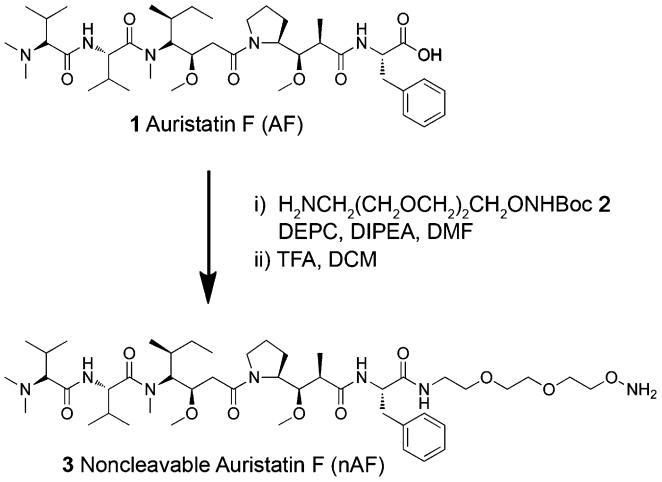

Scheme S1. Structure of AF and nAF linker derivative.

For auristatin-linker synthesis, starting materials, solvents, and reagents were obtained from commercial sources and used as is. Reactions were performed under argon atmosphere. ^{1}H NMR spectra were recorded on Varian Mercury instrument 300 using deuterated chloroform (99.8% D) as solvent. ^{1}H Chemical shift values (δ) are reported in ppm downfield from tetramethylsilane as standard. Mass spectra were measured in positive-mode electrospray ionization (ESI) on Agilent LC/MSD TOF instrument. Thin-layer chromatography was performed on silica gel 60 F_{254} glass plates. Column chromatography was performed using silica gel (35–75 mesh).

Auristatin F (**1**) (1) and noncleavable linker **2** (2), were synthesized as previously described. Synthesis of nAF derivative (**3**) was achieved by amine coupling using **1** and the Boc-protected alkoxy-amine linker **2**, as shown, and subsequently removing the Boc protection using trifluoroacetic acid (TFA).

Compound **3**: DEPC (0.24 mL, 1.56 mmol) and DIPEA (0.5 mL, 2.6 mmol) were added sequentially to a solution of compounds **1** (300 mg, 0.402 mmol) and **2** (117 mg, 0.442 mmol) in DMF (5 mL) at 0 °C, and the mixture was stirred at 0 °C to room temperature for 12 h. The reaction mixture was diluted with DCM, washed with saturated aqueous NH_4Cl, water, dried (Na_2SO_4), filtered, and concentrated in vacuo. Purification of the crude material using column chromatography (silica gel, 4–5% MeOH in DCM) afforded the coupling product (312 mg, 75% yield) as a white solid. ^{1}H NMR ($CDCl_3$, 300 MHz): δ 8.23 (bs, 1H), 7.27–7.21 (m, 5H), 7.17–7.07 (m, 2H), 6.98–6.82 (m, 1H), 4.87–4.81 (m, 2H), 4.21–4.10 (m, 4H), 3.82–3.57 (m, 10H), 3.54–3.27 (m, 4H), 3.08 (s, 6H), 3.00 (s, 3H), 2.57–2.49 (m, 4H), 1.96–1.82 (m, 8H), 1.67–1.52 (m, 4H), 1.43 (s, 9H), 1.07–0.89 (m, 26H). HRMS (ESI): Calculated for $C_{51}H_{90}N_7O_{12}$, 992.6642 $(M+H)^+$; Found, m/z 992.6636.

TFA (0.4 mL) was added to a solution of the above-described coupling product (300 mg, 0.29 mmol) in dry DCM (5 mL) at 0 °C, and the mixture was stirred at this temperature for 12 h. The reaction mixture was then concentrated in vacuo, and washed with Et_2O to give compound **3** (209 mg, 77% yield) as a white solid. HRMS (ESI): Calculated for $C_{46}H_{81}N_7O_{10}$, 892.6045 $(M+H)^+$; Found, m/z 892.6042.

1. Doronina SO, et al. (2008) Novel peptide linkers for highly potent antibody-auristatin conjugate. *Bioconjug Chem* 19:1960–1963.

2. Jones DS, et al. (2001) Synthesis of LJP 993, a multivalent conjugate of the N-terminal domain of β2GPI and suppression of an anti-β2GPI immune response. *Bioconjug Chem* 12:1012–1020.

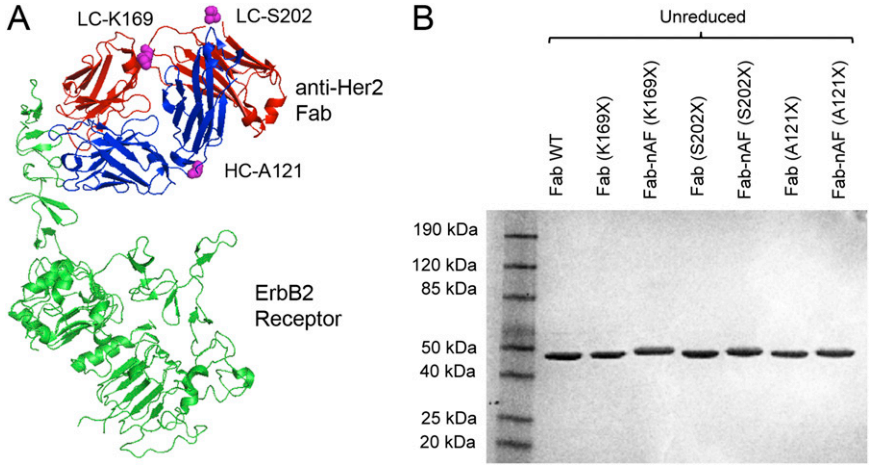

Fig. S1. (*A*) Mutation sites LC-K169, LC-S202, and HC-A121 of anti-Her2 Fab shown with the cocrystalized ErbB2 surface receptor (PDB: 1N8Z). The sites were selected to be distant from the antigen binding site. (*B*) SDS/PAGE analysis of anti–Her2-Fab and Fab drug conjugates. The unreduced Fab is ~48 kDa and the Fab-noncleavable aursitatin conjugates have slightly higher mobility. The 4–12% Tris-Glycine gel (Invitrogen) has Benchmark prestained protein ladder in the first lane and was stained with Coomassie.

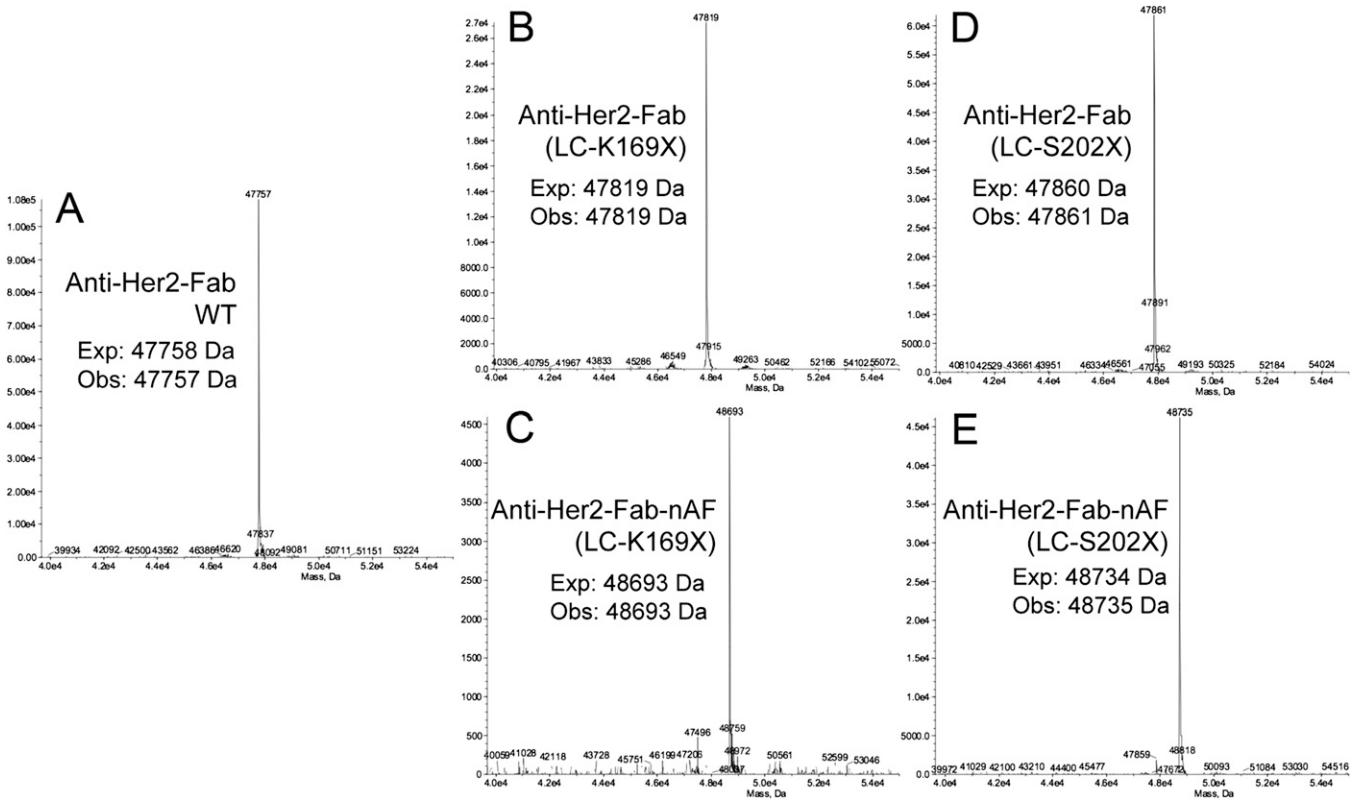

Fig. S2. (*A*) ESI-MS of anti–Her2-Fab wild-type [without *p*-acetylphenylalanine (pAcPhe)]. (*B* and *D*) ESI-MS of the unconjugated LC-K169X and LC-S202X Fab pAcPhe mutants and (*C* and *E*) the mass of the two Fabs conjugated to noncleavable auristatin F (nAF), respectively. The differences between wild-type and the unconjugated mutants are consistent with replacing the respective residue with pAcPhe. Auristatin conjugates are 874 Da larger than the unconjugated Fab.

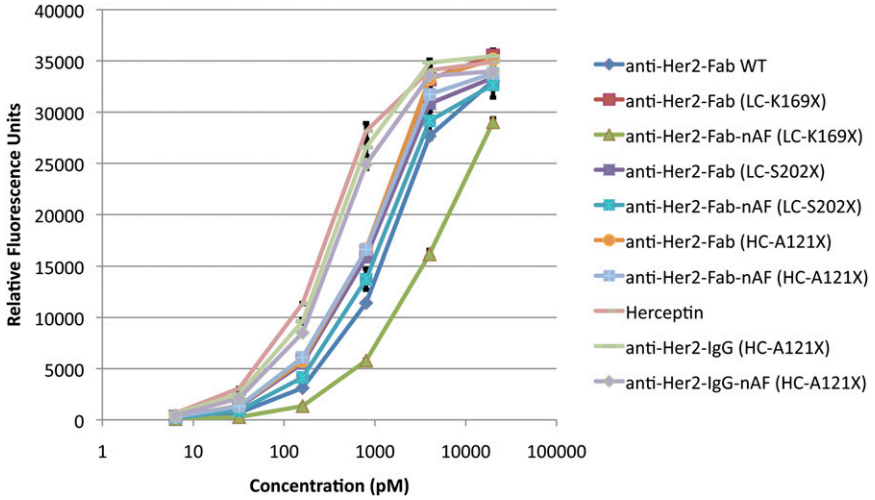

Fig. S3. ELISA of antibody variants and their auristatin conjugates captured by human ErbB2 receptor Fc fusion (R&D Systems) and detected with antihuman κ-HRP (Sigma). All Fabs and their conjugates have similar K_D's (~1 nM), except anti–Her2-Fab(LC-K169X)-nAF, which is likely because of inability of anti–κ-HRP secondary antibody to bind in the same region where the auristatin is conjugated. Herceptin (Genentech), unconjugated mutant IgG and nAF-conjugated IgG have K_D of ~0.3 nM. Error bars represent SD of three replicates.

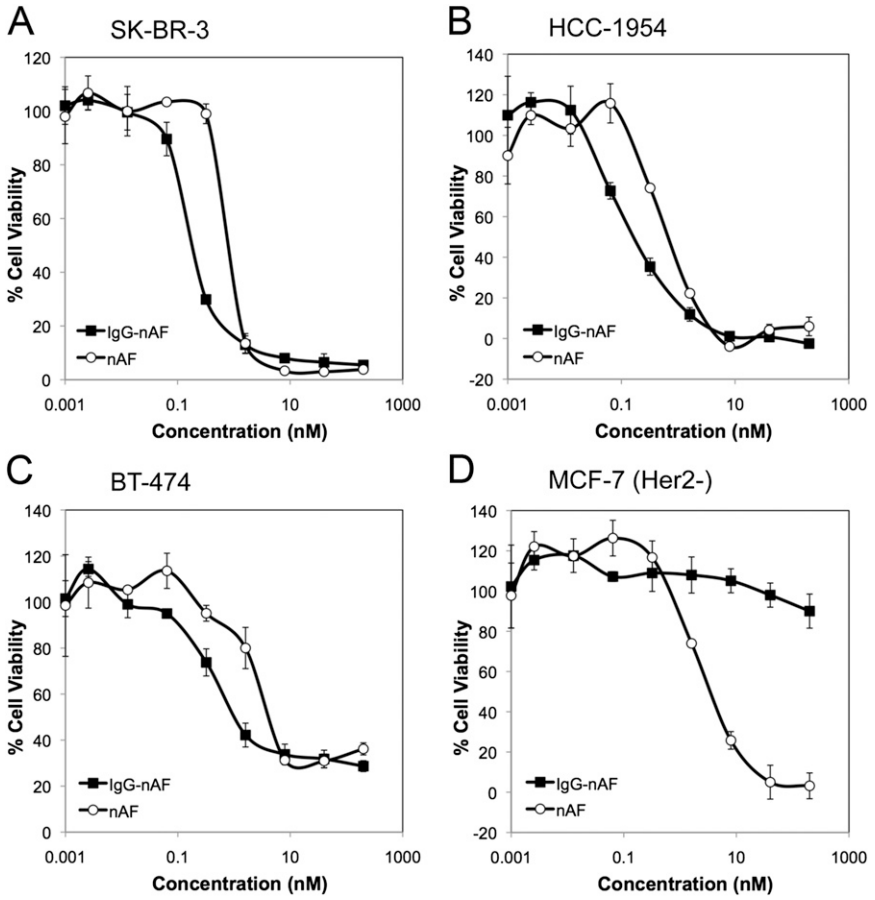

Fig. S4. Cytotoxity of anti–Her2-IgG(HC-A121X)-nAF and unconjugated nAF on $Her2^+$ breast cancer cell lines. (*A*) SK-BR-3 (IgG-nAF EC_{50} 0.17 ± 0.05 nM; nAF EC_{50} 0.82 ± 0.54 nM), (*B*) HCC-1954 (IgG-nAF EC_{50} 0.11 ± 0.22 nM; nAF EC_{50} 0.53 ± 0.27 nM), (*C*) BT-47 (IgG-nAF EC_{50} 0.35 ± 0.20 nM; nAF EC_{50} 2.0 ± 6.1 nM). (*D*) MCF-7, considered $Her2^-$ breast cancer cells, showed little cytotoxicity due to IgG-nAF, despite having an EC_{50} of 3.2 ± 2.0 nM for nAF alone. Error bars represent SD of three replicates.

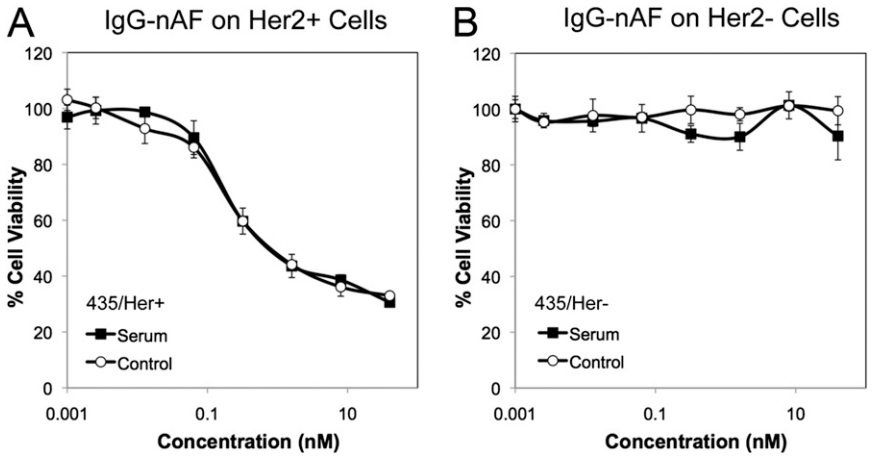

Fig. S5. Stability of anti–Her2-IgG(HC-A121X)-nAF after incubating 3 d in mouse serum at 37 °C. The compounds were diluted to assay concentrations and normal cytotoxicity assays were conducted. The "Control" sample was mixed with mouse serum in similar concentrations immediately before use in the cytotoxicity assay. (*A*) MDA-MB-435/Her2^{+} cells were used to test for decreases in antibody-drug conjugate (ADC) activity, and (*B*) MDA-MB-435/Her2^{-} cells were used to test for cleavage of the small molecule that would cause passive cytotoxicity. Error bars represent SD of three replicates.

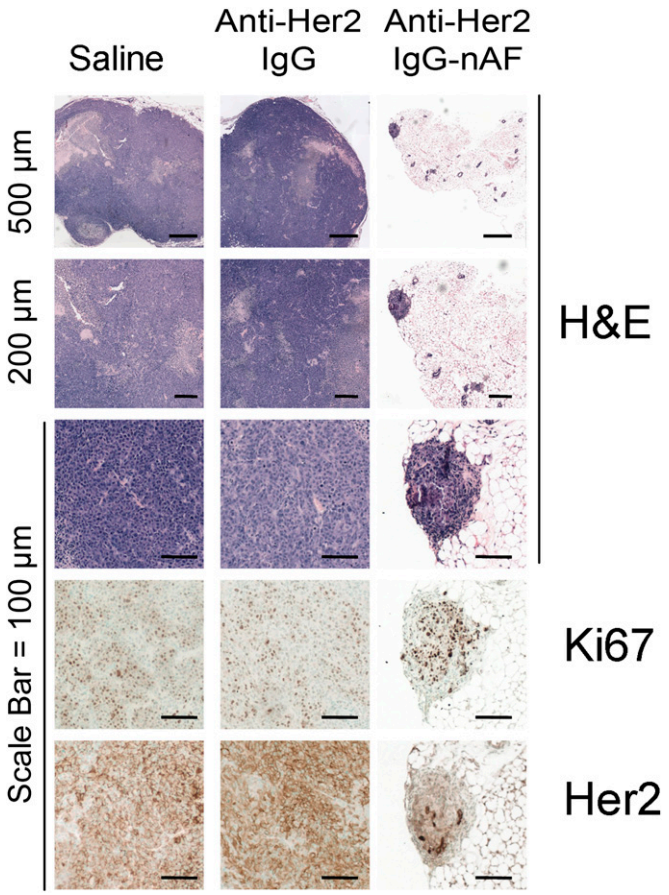

Fig. S6. Effect of anti–Her2-IgG(HC-A121X)-nAF on mammary tumors in vivo. Histological (H&E staining), proliferative (Ki67), and Her2 expression (Her2) analysis was conducted on tumors extracted 29 d after mammary fat pad injection of 2.5×10^5 MDA-MB-435/Her2^{+} cells and a single 5-mg/kg dose of anti–Her2-IgG-nAF, anti–Her2-IgG, or DPBS at day 8. For each group, one of eight representative tumors is shown.

Table S1. Summary of EC_{50} values and SD for cytotoxicity assays of the various cell lines and compounds

Figure	Cell line	Compound	EC_{50} (nM)	SD
Fig. 2*A*	MDA-MB-435/Her2^{+}	IgG(HC-A121X)-nAF	0.37	0.38
		Fab(LC-K169X)-nAF	21.3	13.7
		IgG(HC-A121X)	>200	
		nAF	1.5	1.7
Fig. 2*B*	MDA-MB-435/Her2^{-}	IgG(HC-A121X)-nAF	>200	
		Fab(LC-K169X)-nAF	>40	
		IgG(HC-A121X)	>200	
		nAF	0.92	2.4
Fig. 2*C*	SK-BR-3	Fab(LC-K169X)-nAF	8.3	3.4
		Fab(LC-S202X)-nAF	2.1	2.8
		Fab(HC-A121X)-nAF	1.8	0.33
Fig. S4*A*	SK-BR-3	IgG(HC-A121X)-nAF	0.17	0.05
		nAF	0.82	0.54
Fig. S4*B*	HCC-1954	IgG(HC-A121X)-nAF	0.11	0.22
		nAF	0.53	0.27
Fig. S4*C*	BT-474	IgG(HC-A121X)-nAF	0.35	0.20
		nAF	2.0	6.1
Fig. S4*D*	MCF-7	IgG(HC-A121X)-nAF	>40	
		nAF	3.2	2.0
Fig. S5*A*	MDA-MB-435/Her2^{+}	IgG(HC-A121X)-nAF (Serum)	0.24	0.11
		IgG(HC-A121X)-nAF (Control)	0.21	0.10
Fig. S5*B*	MDA-MB-435/Her2^{-}	IgG(HC-A121X)-nAF (Serum)	>40	
		IgG(HC-A121X)-nAF (Control)	>40	

Table S2. Pharmacokinetic parameters for anti–Her2-IgG(HC-A121X)-nAF and anti–Her2-IgG(HC-A121X) (mean ± SD)

	T1/2 (half-life) (h)	$AUC_{(inf)}$ (h·ng/mL)	Clearance (mL/h/kg)	Vss (mL/kg)
Anti–Her2-IgG(HC-A121X)-nAF	183 ± 16	3,213,000 ± 304,000	0.31 ± 0.03	81 ± 5
Anti–Her2-IgG(HC-A121X)	224 ± 82	3,632,000 ± 1,052,000	0.3 ± 0.11	86 ± 13

The serum concentrations for time points from 6 to 336 h were analyzed using WinNonlin PK/PD Modeling and Analysis software (PharSight). $AUC_{(inf)}$, area under the curve projected to infinity; Vss, volume of distribution. Parameters are calculated separately for each rat. Values in the table represent the mean of five different rats. Error is SD.